Ship hull in-water cleaning and its effects on fouling-control coatings

(article starts on next page)

Ship hull in-water cleaning and its effects on fouling-control coatings

Dinis Reis Oliveira & Lena Granhag

View supplementary material ☐

Published online: 13 May 2020.

Submit your article to this journal ☐

Article views: 362

View related articles ☐

View Crossmark data ☐

Taylor & Francis
Taylor & Francis Group

Ship hull in-water cleaning and its effects on fouling-control coatings

Dinis Reis Oliveira [ID] and Lena Granhag [ID]

Department of Mechanics and Maritime Sciences, Chalmers University of Technology, Gothenburg, Sweden

ABSTRACT

Today, ship hull fouling is managed through fouling-control coatings, complemented with in-water cleaning. During cleaning, coating damage and wear must be avoided, for maximum coating lifetime and reduced antifoulant release. When possible, cleaning should target early stages of fouling, using minimal forces. However, such forces, and their effects on coatings, have not yet been fully quantified. In this one-year study, minimal cleaning forces were determined using a newly-designed immersed waterjet. The results show that bi-monthly/monthly cleaning, with maximum wall shear stress up to $\sim 1.3\,kPa$ and jet stagnation pressure $\sim 0.17\,MPa$, did not appear to cause damage or wear on either the biocidal antifouling (AF) or the biocide-free foul-release (FR) coatings. The AF coating required bi-monthly cleanings to keep fouling to incipient slime (time-averaged results), while the FR coating had a similar fouling level even without cleaning. The reported forces may be used in matching cleaning parameters to the adhesion strength of the early stages of fouling.

Introduction

Marine fouling-control coatings are currently used on underwater surfaces of ships and stationary marine structures for the prevention of biofouling. Besides coatings, in-water cleaning, by divers or remotely operated vehicles (ROVs), may become necessary (IMO 2011). However, the relationship between cleaning forces and the subsequent performance of marine coatings has not been fully addressed in a quantitative way (Oliveira and Granhag 2016).

Ships' hull and propeller fouling leads to increased roughness on these surfaces, which is responsible for increased hydrodynamic hull resistance and reduced propeller efficiency. Thus, biofouling leads to higher power requirement for propelling the ship at a given speed, which means significantly higher fuel consumption and emission of air pollutants and greenhouse gases (Schultz 2007; Kellett et al. 2015). On the other hand, commonly used methods for preventing fouling may also lead to significant environmental burdens, such as (1) chemical pollution due to release of antifoulants from ship hull coatings, which may be exacerbated by in-water cleaning (Earley et al. 2014), and (2) the risk of spread of non-indigenous species

from fouled hulls, as a result of depleted or ineffective hull coatings, or from uncaptured waste during in-water cleaning on such hulls (Morrisey et al. 2013).

The current paper aims to address the knowledge gap in the effect of quantified cleaning forces on the subsequent performance of ship hull coatings. The release of antifoulants as a function of cleaning frequency is also studied, in parallel with performance assessment of a biocide-free foul-release (FR) coating.

In-water maintenance

In-water hull and propeller maintenance traditionally follows a reactive approach, in which surfaces are cleaned once a certain degree of fouling is detected (Malone 1980; Naval Sea Systems Command 2006). Conventional hull cleaning is conducted by divers using rotating-brush carts, or using ROVs equipped with rotating brushes or waterjets (Morrisey and Woods 2015). Alternatively, preventive maintenance approaches have also been suggested, such as hull grooming on US Navy vessels, consisting in frequent and gentle wiping of the hull (Tribou and Swain 2010; Tribou and Swain 2017), and continuous

prevention methods, such as aeration (Menesses et al. 2017) or ultrasound transducers (Park and Lee 2018).

In-water cleaning aims at removing fouling, optimally without damage or wear to the underlying coating. Damage and wear may result in shortening of the coatings' lifetime (Malone 1980; Holm et al. 2003) and lead to a temporary increase in release of antifoulants (Earley et al. 2014). Thus, for mitigating adverse effects on coatings and the marine environment, it has been suggested that cleaning forces be minimized, by matching forces to the adhesion strength of fouling (Oliveira and Granhag 2016).

Previous research related to in-water cleaning (reactive approach) and hull grooming (preventive/proactive approach) on modern marine coatings essentially focused on at least one of the following three aspects: (a) adhesion strength of fouling, particularly for comparison between different FR coatings (e.g. Swain and Schultz 1996; Cassé and Swain 2006; Zargiel and Swain 2014); (b) effects of cleaning and hull grooming on the composition of fouling communities and their hydrodynamic drag (Zargiel and Swain 2014; Hunsucker et al. 2018); and (c) the effects of cleaning and hull grooming on the environmental load of antifoulants from biocidal antifouling (AF) coatings (Schiff et al. 2004; Earley et al. 2014; Tribou and Swain 2017). Furthermore, with the phase-out of tributyl tin (TBT) as a harmful antifoulant and other regional restrictions on use of biocides, increasing attention has been devoted to biocide-free alternatives (Lejars et al. 2012; Gittens et al. 2013). In spite of some uptake of biocide-free solutions, biocidal AF coatings still represent at least 90% of the hull coating market for commercial vessels (Lindholdt, Dam-Johansen, Olsen, et al. 2015). Therefore, research on the effects of in-water cleaning on biocidal coatings is still highly relevant, as required for assessing and minimizing the risks posed by such maintenance practices (Scianni and Georgiades 2019).

Previous studies demonstrated that some aggressive cleaning techniques can significantly increase biocide emissions, namely copper compounds, from recreational vessels (Schiff et al. 2004; Earley et al. 2014). These studies applied the US Navy's dome method for measuring biocide release rates. In another study, Tribou and Swain (2017) determined the equivalent biocide loss rate from the AF coating Interspeed® BRA640, using measurements of dry film thickness (DFT) and the copper content in leachate samples. These authors found significant differences in wear between groomed and ungroomed panels. However, none of these studies reported on shear and normal forces exerted by their cleaning tools at the wall surface. Quantification of these forces would enable translation of results into recommended cleaning forces for commercial in-water cleaning, enabling clearer standards for developers of hull cleaning devices, in-water cleaning operators, and authorities responsible for issuing approvals on in-water maintenance of ship hulls.

Quantification of cleaning forces

Methods for testing adhesion strength, i.e. the forces required to remove fouling from different coatings, have been available at least since the 1990s. Fouling is usually grouped into macro- or microfouling, respectively for larger (typically > 1 mm) or smaller-sized individuals. For macrofouling, more specifically for acorn barnacles, a standard method for adhesion strength in shear is available (ASTM D5618.5618 1994). This method has also been modified to measure the adhesion strength of other hard fouling organisms, such as oysters and tubeworms (Kavanagh et al. 2001). For microfouling, hydrodynamic methods have been developed, including the calibrated waterjet (Swain and Schultz 1996), and the turbulent channel flow apparatus (Schultz et al. 2000). Modified and automated versions of the calibrated waterjet have also been used for adhesion-strength comparison between different FR coatings (Finlay et al. 2002; Cassé et al. 2007). However, caution must be exercised in comparing results from different studies, since the reported forces, typically in units of force per unit area, may not correspond to the same definition of adhesion strength (Oliveira and Granhag 2016). In ASTM D5618 standard method, barnacle adhesion strength is calculated based on the exerted shear force using a handheld gage, which is divided by the area of the barnacle's basal plate (ASTM D5618.5618 1994). Instead, in hydrodynamic methods for microfouling, adhesion strength is reported as hydrodynamic shear stress exerted on a smooth wall (Schultz et al. 2000; Finlay et al. 2002). Also, discrepancies between lab tests and field performance of FR coatings on hulls have been reported, which were attributed to different modes of adhesion failure resulting from different force components being applied on the fouling (Larsson et al. 2010).

Previous studies on the effects of cleaning and hull grooming on AF coatings focused on biocide release rates (Schiff et al. 2004; Earley et al. 2014), and the wear or polishing rate of the top coating (Hearin et al. 2015; Tribou and Swain 2017). However, there are limited amounts of data available for AF coatings

on the adhesion strength of fouling (Oliveira and Granhag 2016). To the authors' knowledge, adhesion strength on AF coatings was only reported for barnacle fouling on Interspeed® BRA640 (Tribou and Swain 2015), and no data are currently available on the adhesion strength of microfouling on AF coatings. This lack of data on AF coatings is probably due to concerns about erosion that may occur during water-jet testing on AF coatings (Zargiel and Swain 2014) or the occurrence of cohesive failure of macrofouling on AF coatings. For example, barnacle shells may break instead of complete removal of their base plates (Oliveira and Granhag 2016). Nevertheless, the adhesion strength of microfouling on AF coatings is currently defined as the amount of force per unit area required to remove fouling with negligible wear to the biocide-containing top coating.

In order to adequately quantify cleaning forces, waterjet adhesion-strength testing was currently selected as the cleaning method. The present setup differs from previous water-in-air jet designs (Swain and Schultz 1996; Finlay et al. 2002; Cassé et al. 2007), as the present results are instead obtained using an *immersed* water jet. This setup enables application of semi-empirical formulae for estimation of wall surface forces, which are based on geometrical parameters and fluid properties (Oliveira et al. 2019).

Materials and methods

Test panels and coatings

Hull steel panels (AB Gotenius Varv, Gothenburg, Sweden), dimensions $0.180 \times 0.240 \times 0.006$ m (Figure 1), were used as substrata for applying three separate coating systems: an antifouling copper-containing coating (AF), a biocide-free silicone foul-release coating (FR), and an anti-corrosive epoxy primer (E), lacking any fouling-control properties and thus providing an unprotected surface for evaluation of local fouling pressure. All panels were coated on both the front- and backsides. All thickness values given in this sub-section are nominal, as per paint specification. Triplicate panels were used under each cleaning treatment.

The first set of panels was coated with an antifouling product, denoted here as AF panels. According to product documentation, the top coating PPG Sigma Ecofleet® 290 is a rosin-based self-polishing coating, designed for ocean-going vessels, i.e. for medium- to high-activity vessels. This coating contains copper oxide (Cu_2O) as the main biocide, and zineb (zinc ethylene bis-dithiocarbamate) as the co-biocide, or booster biocide. An airless spray technique was used by ship-repair
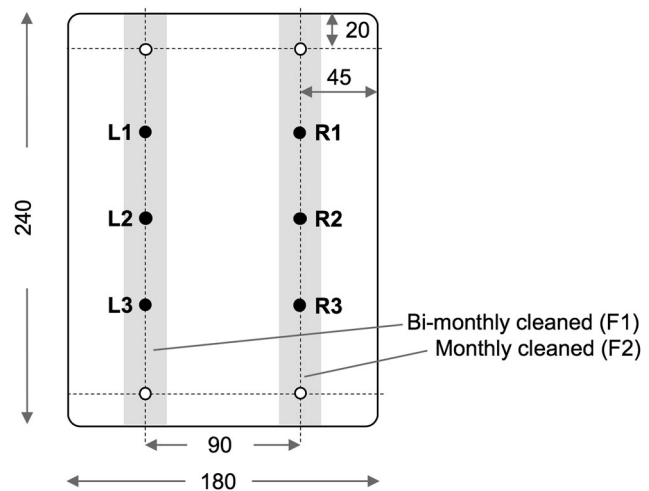

Figure 1. Dimensions of hull steel panels, with cleaning paths marked in grey, i.e. theoretical area covered by maximum wall shear stress. Locations for dry film thickness measurements are labelled L1 – R3.

yard workers (AB Gotenius Varv, Gothenburg, Sweden), according to the manufacturer's specifications (Sigma Färg, Mölndal, Sweden). The red-brown coloured PPG Sigma Ecofleet® 290 was applied at a specified dry film thickness DFT $\sim$100 μm, over a black tie-coat PPG Sigmacover® 555, DFT $\sim$75 μm, with an underlying anti-corrosive primer PPG Sigmaprime® 200, DFT $\sim$250 μm (two layers, $\sim$125 μm each).

A second set of panels was coated with a biocide-free foul-release coating, denoted here FR panels. The top coating was PPG Sigmaglide® 1290, a silicone-based FR coating. The coating system was applied by the paint manufacturer (PPG Research Center Amsterdam, the Netherlands). The red-brown coloured PPG Sigmaglide® 1290 was applied at a specified DFT $\sim$180 μm, over a black layer of PPG Sigmaglide® 790, DFT $\sim$150 μm, with an underlying anti-corrosive primer PPG Sigmaprime® 700, DFT $\sim$150 μm, and a first layer of primer PPG Sigmaprime® 200, DFT $\sim$150 μm.

A third and final set of panels, denoted here E panels, was kept with only the anti-corrosive epoxy primer, PPG Sigmaprime® 200, DFT $\sim$300 μm (two layers, $\sim$150 μm each). These were used for evaluating local fouling pressure on an unprotected surface.

Field test site

The test site was located in the Saltholmen marina, Kattegat Sea, west coast of Sweden (57.659897 N 11.837372 E). The marina is located $\sim$3.5 km south

from the Port of Gothenburg, across the mouth of the Göta River.

A 40-m long floating platform was selected for deploying all test panels under similar light exposure and hydrodynamic conditions (local almost-static flow). Deployment depth was kept constant for all panels, at ∼ 0.5 m, and sea depth at the site ranged between 1.6 and 3.4 m, depending on the tide (SMHI. 2019). The SW-facing side of the platform was used, for maximizing exposure to sunlight. At this latitude, daylight hours vary between ∼7 h in December (winter) and ∼18 h in July (summer). Even though the location is characterized by seasonal fouling, good exposure to sunlight combined with idle immersion maximized the challenge for prevention of fouling (Woods Hole Oceanographic Institute 1952).

Environmental parameters were monitored, including surface seawater temperature, salinity, pH and local currents. The temperature ranged between 0.4 °C in February 2019 and 23.4 °C in July 2018, averaging 8.8 ± 6.9 °C (average ± SD, 4-h logging interval), salinity 18.8 ± 4.2 ppt (monthly measurements), and pH 8.1 ± 0.1 ($n = 14$ observations in July 2018). Additionally, the hydrodynamic conditions were sampled in February 2019 (winter) using an acoustic Doppler velocimeter, ADV (Nortek Vector 300 m, Nortek BV, The Netherlands). At a distance of ∼10 cm from the panels, maximum instant velocity magnitude did not exceed 0.30 m s^{-1} (∼0.6 knots).

Adhesion strength

An immersed waterjet system was built, based on previous designs for calibrated waterjets (Swain and Schultz 1996; Finlay et al. 2002). Compared to previous versions, two main modifications were introduced in the current waterjet system: (1) immersion of both the waterjet and test panel, and (2) direct measurement of the flowrate issuing from the nozzle. These two modifications allowed for estimation of forces exerted on the panel, as detailed below.

As illustrated in Figure 2, the immersed waterjet was driven by compressed air from a SCUBA tank. Tank #1 contained compressed air at up to 20 MPa, which was regulated down to ∼0.8 MPa by means of a diving 'first stage' regulator. The low-pressure air was then tapped to the top of SCUBA tank #2, which was pre-filled with filtered seawater (textile mesh with 1-mm spacing). The second tank was perforated at the bottom, allowing seawater to flow to the nozzle. Before the nozzle, a valve and a flowmeter (rotameter) were used for regulating the flowrate down to the desired value.

An immersion tank with capacity of ∼30 l was used ($x \times y \times z$-dimensions $0.88 \times 0.41 \times 0.08$ m), with constant depth being kept by allowing overflow at an 8-cm weir (Figure 2). Besides avoiding sample desiccation, an immersed jet enables the estimation of wall surface forces from empirical formulae. Thus, for immersed non-cavitating waterjets, stagnation pressure p_s (N m^{-2}) and maximum wall shear stress $\tau_{w,max}$ (N m^{-2}) are estimated as (Oliveira et al. 2019):

$$p_s = 27.7 \frac{\rho u_0^2}{(H/D)^2}, \text{ at r/H} = 0 \qquad (1)$$

$$\tau_{w,max} = 5.22 \frac{\rho u_0^2 Re^{-0.3159}}{(H/D)^2}, \text{ at r/H} \approx 0.1 \qquad (2)$$

where ρ is seawater density (kg m^{-3}), u_0 is the mean seawater velocity through the nozzle (m s^{-1}), H is the nozzle standoff distance (m), Re is the Reynolds number based on nozzle inner diameter D (m), and r is the radial distance from the jet impingement (m). These formulae were derived for immersed jets (Oliveira et al. 2019), and therefore do not apply to water-in-air jets used in previous studies (Swain and Schultz 1996; Finlay et al. 2002).
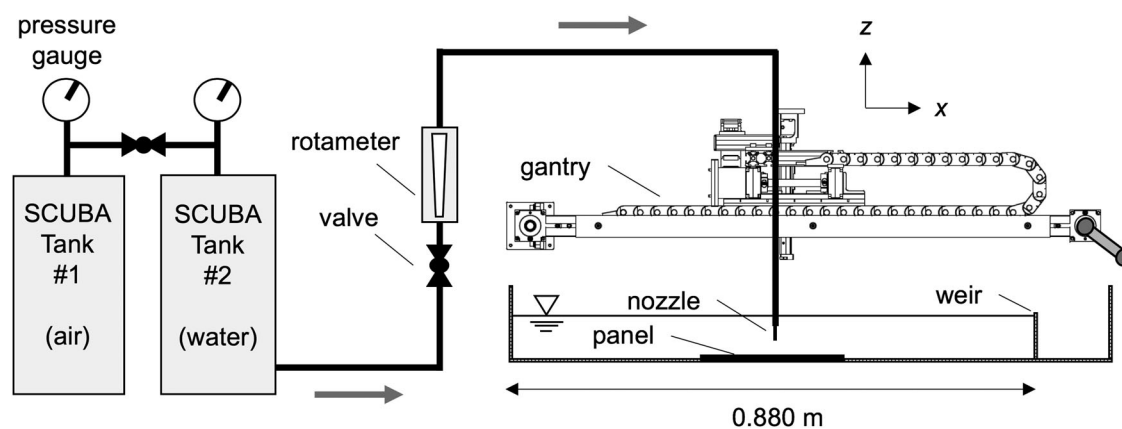

Figure 2. Schematic representation (lateral view) of the immersed waterjet.

The selected nozzle was a 38-mm long pipe nozzle, with an inner diameter $D = 1.6$ mm and a contraction ratio of 7:1 (Nordson EFD, RI, USA). The nozzle was positioned at a standoff distance $H = 15.625 \times D = 0.025$ m. This was achieved by manual adjustments on the z axis of the gantry positioning system (Macron Dynamics, NY, USA) fitted above the panel (Figure 2). The flowrate through the nozzle, and consequently the fluid velocity through the nozzle u_0 (Equations 1 and 2), was controlled using a water valve and rotameter, added before the nozzle (Figure 2). The rotameter had a range 0.25 – 3.00 l min^{-1}, with an accuracy of $\pm$ 0.15 l min^{-1} (Kytola Instruments, Muurame, Finland). The sensitivity of the surface forces (Equations 1 and 2) to the accuracy of the flowrate and nozzle standoff distance are presented in the Supplemental materials, where final errors in the surface forces are comparable to those introduced by a limited resolution in flowrate steps, as further dealt with below in this subsection.

The nozzle translation speed in the x direction, controlled using the gantry system (Figure 2), was kept constant for FR panels (0.01 m s^{-1}). For AF panels, this nozzle translation speed was introduced as a variable for studying the cleaning and coating erosion process in more detail (0.01, 0.02 or 0.03 m s^{-1}). For each nozzle passage, the nozzle was set in motion over the sample by actuation of the x-axis belt of the gantry positioning system (Figure 2), using a manually-operated actuation handle connected to the x-axis belt. The rate of revolution of the manual handle was calibrated against the corresponding travel speed along the x axis. Thus, each translation speed was achieved by matching the speed of rotation of the manually-operated handle (intervals of 1/6 of a revolution were used for convenience) to the rhythmic acoustic signal from a digital metronome (34, 68 and 103 beats min^{-1} were used for 1/6 of a revolution of the manual handle, corresponding to translation speeds along the x axis of 0.01, 0.02 and 0.03 m s^{-1}, respectively). The experimental setup was thus made simpler and more portable, by avoiding the use of automation controllers and power supplies in the field.

Panels were cleaned along a 25-mm wide path using the immersed waterjet. The theoretical cleaning path, shaded grey in Figure 1, was centred with reference to the centreline of each half of the panel. This cleaning path was achieved by five parallel passes of the nozzle, spaced by 5-mm travels in y axis of the gantry positioning system (Figure 2). The selected spacing covers the cleaning area with maximum wall shear stress, which is expected at a radius $r \approx 0.1$ $H = 2.5$ mm from the jet impingement (Equation 2).

Adhesion strength was evaluated by translating the jet over the panels, as described above. Each run started with the lowest flowrate, and proceeded with stepwise increases in flowrate (five parallel nozzle passes per flowrate step) until the surface was visually clean (bare coating) or the maximum flowrate was reached (Swain and Schultz 1996; Hunsucker and Swain 2016). When the surface was already visually clean from the start, panels were still subjected to waterjet cleaning at the minimum flowrate, following a proactive maintenance approach.

Flowrate Q steps are given in Table 1, along with estimated surface forces at the wall $\tau_{w,max}$ and p_s, which were calculated based on Equations 1 and 2. For a standoff distance $H = 25$ mm, the maximum wall shear stress $\tau_{w,max}$ ranged between $\sim$25 and $\sim$530 Pa. For each run, forces were calculated using seawater properties, according to the temperature of the cleaning fluid (measured on each run) and salinity (measured daily). The condition of the nozzle was carefully checked at the start of the measurements, in order to detect any clogging, and visual checks were performed on each run, in order to detect any flow anomalies (cavitation or air bubbles issuing from the nozzle). Direct measurement of surface forces would be needed in order to validate the estimated forces (Equations 1 and 2) and verify the accuracy of the apparatus over time, but these measurements were not presently included. Future development of surface-force characterisation, in particular of accurate wall shear force measurements, would be required. Presently, the estimation of force based on Equations 1 and 2 was deemed sufficiently accurate for the current aim.

Table 1. Maximum wall shear stress $\tau_{w,max}$ and stagnation pressure p_s at the wall (Equations 1 and 2, respectively), as a function of flowrate Q through a pipe nozzle with $D = 1.6$ mm, at standoff distances $H = 25$ mm and 16 mm.

Q [l min^{-1}]	u_0 [m s^{-1}]	Re [-]	$\tau_{w,max}$ [Pa]		p_s [Pa]	
			$H = 25$ mm	$H = 16$ mm	$H = 25$ mm	$H = 16$ mm
0.50 (*)	4.14	4.88E + 03	26	63	2.00E + 03	4.89E + 03
1.00	8.29	9.75E + 03	83	202	8.01E + 03	1.95E + 04
1.30 (*)	10.78	1.27E + 04	129	315	1.35E + 04	3.30E + 04
1.50	12.43	1.46E + 04	164	401	1.80E + 04	4.40E + 04
1.80 (*)	14.92	1.76E + 04	223	545	2.59E + 04	6.33E + 04
2.00	16.58	1.95E + 04	266	650	3.20E + 04	7.82E + 04
2.50 (*)	20.72	2.44E + 04	388	947	5.00E + 04	1.22E + 05
3.00	24.87	2.93E + 04	527	1287	7.21E + 04	1.76E + 05

(*) – These flowrate steps were only used on the first and second cleaning events (May and June 2018). Surface forces are given for seawater at 10 °C and salinity 35 ppt ($\rho = 1026.9$ kg m^{-3}; $\nu = 1.3602 \times 10^{-6}$ m^2 s^{-1}).

It should be noted that the first two cleaning events were ran with a higher number of flowrate steps (Table 1). From the third monthly cleaning event onwards ($t \geq 91$ days), the intermediate flowrate steps (0.5, 1.3, 1.8 and 2.5 l min^{-1}) had to be omitted due to time restrictions (see also sensitivity analysis in the Supplemental materials, which shows that input-variable errors are comparable to flowrate-step resolution errors). Finally, on the last three cleaning events, starting from $t = 307$ days, the standoff distance of the nozzle (H) was lowered in an attempt to remove tenacious biofilms that had formed on all panels (Table 2). Thus, since surface forces increase with the inverse-square of the standoff distance H (Equations 1 and 2), by lowering H from 25 to 16 mm the maximum wall shear stress was increased from $\sim$530 to $\sim$1,300 Pa at a maximum flowrate of 3.0 l min^{-1} (Table 1). Also according to Equation 2, a decrease in H requires a smaller gap between passes of the waterjet (y axis in Figure 2), which therefore was reduced from 5- to 3-mm travels, increasing also the number of passes from five to nine passes, for covering a cleaning path of at least 25 mm.

Deployment-and-cleaning schedule

The deployment-and-cleaning schedule is given in Table 2, where t corresponds to the number of days since initial deployment. All of AF and FR coated panels were deployed simultaneous on 4 April 2018, after approximately two weeks paint drying time, and these remained immersed under local almost-static flow conditions throughout the entire study. For evaluating the local fouling pressure, anti-corrosive epoxy (E) coated panels were deployed and collected on a monthly basis. All panels were deployed in groups of two or three panels on each rack, with randomized spatial arrangement along the floating platform. Randomized order was also used when cleaning with the waterjet, which was performed within a maximum of two consecutive days.

Cleaning with the immersed waterjet took place at two different frequencies, on a bi-monthly (frequency F1) or monthly basis (F2), as indicated in Table 2. Panels cleaned bi-monthly/monthly were divided vertically into two halves, corresponding to left and right side. Each half was cleaned bi-monthly (F1) or monthly (F2), as exemplified in Figure 1. The use of the same panel for both cleaning frequencies aimed at reducing variability due to possible panel-to-panel differences in quality of paint application. Cleaning of one half of the panel is not expected to impact the other half of the panel, considering that shear forces experienced at that distance ($r \cong 70$ mm $= 2.8$ H) is less than one order of magnitude compared to the maximum wall shear stress, $\tau_{w,max}$ (Beltaos and Rajaratnam 1974). This assumption was confirmed by verifying that there was no significant change in fouling rating and percentage cover for the non-cleaned half of the panel upon cleaning the other half.

Throughout this paper, different cases and cleaning treatments are identified by codes for top coating (AF – antifouling, FR – foul-release, E panels – epoxy anti-corrosive coating), nozzle translation speed (S1: 0.01 m s^{-1}; S2: 0.02 m s^{-1}; S3: 0.03m s^{-1}), and cleaning frequency (F0 – no cleaning, F1 – bi-monthly, and F2 – monthly). For instance, case AFS2F2 corresponds to AF panels, cleaned with a nozzle translation speed of 0.02 m s^{-1} (S2), on a monthly basis (F2).

Fouling rating

The level of fouling observed on immersed panels was rated based on the US Naval Ships' Technical Manual

Table 2. Cleaning schedule, with indication of nozzle standoff distance H used on each date.

Month	t [days]	Panel deployment	Cleaning events on AF and FR panels		H [mm]
			Bi-monthly (F1)	Monthly (F2)	
2018 Apr	0	E, AF, FR			
2018 May	29	E		X	25
2018 Jun	61	E	X	X	25
2018 Jul	91	E		X (*)	25
2018 Aug	119	E	X (*)	X (*)	25
2018 Sept	154	E		X (*)	25
2018 Oct	183	E	X (*)	X (*)	25
2018 Nov	215	E		X (*)	25
2018 Dec	245	E	X (*)	X (*)	25
2019 Jan	274	E		X (*)	25
2019 Feb	307	E	X (*)	X (*)	16
2019 Mar	334	E		X (*)	16
2019 Apr	364	–	X (*)	X (*)	16

(*) Intermediate flowrate steps (Table 1: 0.5, 1.3, 1.8 and 2.5 l min^{-1}) were only used on the first and second cleaning events (May and June 2018). Key: AF – antifouling coating; FR – foul-release coating; E – epoxy anti-corrosive primer; F1-F2 – code for cleaning frequency.

fouling rating, fr_{NSTM}, which is summarized in Table 3 (Naval Sea Systems Command 2006). This fouling rating relies on visual inspection, with different types of fouling ranging from a minimum $fr_{NSTM} = 0$, i.e. a foul-free surface, and up to a maximum $fr_{NSTM} = 100$, i.e. all forms of fouling present. Fouling is also grouped into two main types: 'soft' fouling ($10 \leq fr_{NSTM} \leq 30$), including 'slime' (biofilm), 'grass' (macroalga), or other colonies without a calcareous shell; and 'hard' fouling ($40 \leq fr_{NSTM} \leq 90$), i.e. animal fouling forming calcareous shells, typically barnacles and tubeworms. This scale has been in use by the US Navy for decision-making on in-water maintenance (Naval Sea Systems Command 2006; Schultz et al. 2011). Additionally, this scale has been associated with propulsion power penalties for representative hull conditions (Schultz 2007; Schultz et al. 2011; Demirel et al. 2017), further confirmed by other authors as giving an approximate first estimate for such penalties (Lindholdt, Dam-Johansen, Yebra, et al. 2015).

The US Navy's fouling rating was applied in this study, with the following two additions. The first addition consisted of accounting encrusting bryozoans under the same category as tubeworms ($fr_{NSTM} = 40$), since encrusting bryozoans were missing from the original scale (Table 3), as already noted by Donnelly et al. (2019). Additionally, juvenile barnacles ≤ 1 mm in diameter were considered as microfouling, and thus included under $fr_{NSTM} = 20$, i.e. advanced slime.

Visual inspection of panels resulted in a variable number of fr_{NSTM} ratings detected on each half panel. The percentage cover was then estimated visually for each of these fr_{NSTM} values, through comparison with standard extent diagrams from ASTM D6990-05 (2005). No overlapping was allowed, i.e. the maximum total percentage cover was 100%. Edge effects were discounted from the analysis by excluding 3-cm margins. Finally, fr_{NSTM} values, and their corresponding percentage cover, were combined into a mean value, given as an areal mean for each half panel as:

$$mean(fr_{NSTM}) = \sum_{i=1}^{N} \frac{fr_{NSTM,i} \times (\%cover)_i}{100} \quad (3)$$

where N is the total number of visible fouling ratings on a given half panel. Further, time averages of fouling rating were calculated using the trapezoidal rule:

$$\overline{mean(fr_{NSTM})} = \sum_{i=1}^{n-1} \frac{mean(fr_{NSTM})_{i+1} + mean(fr_{NSTM})_i}{2} \times \frac{t_{i+1} - t_i}{t_n - t_1} \quad (4)$$

where t is the elapsed time since deployment ($t_1 = 0$ days), and n is the total number of points in time.

Polishing rate mass-balance method

In order to determine biocide release rates from the AF coated panels as a function of cleaning treatment, dry film thickness (DFT) was measured before and after deployment, both under dry conditions. The method is appropriate for coatings that undergo polishing, namely ablative, self-polishing or hybrid coatings, assuming that biocide release is well correlated to the loss in paint thickness (Finnie 2006).

A magnetic probe was used for measuring DFT, Positector® 6000 FNS3 (DeFelsko Corporation, Ogdensburg, NY, USA). This probe has an accuracy of $\pm 2 \mu m$, added by 1% of the actual reading. Probe calibrations were performed by zeroing with a reference ferrous plate, followed by a two-point calibration with certified plastic shims (DeFelsko Corporation, Ogdensburg, NY, USA). DFT measurements ($n = 9$ repeats) were taken on three mapped positions on each half panel, which could be traced back using a template (Figure 1). Measurement positions were evenly spread along the cleaning path of the immersed waterjet, as indicated in Figure 1 by positions L1 to R3.

By the end of the study, panels were left to dry indoors for seven days. Further drying time did not alter the results. The amount of polishing $E_i - E_t$ was

Table 3. US Naval Ships' Technical Manual fouling rating, fr_{NSTM} (Naval Sea Systems Command 2006).

fr_{NSTM} [-]	Type	Hull fouling condition
0	Undetectable	Foul-free surface.
10	Soft	Incipient slime, visible underlying paint/metal surface.
20	Soft	Advanced slime, obscured underlying paint/metal surface. Juvenile barnacles ≤ 1 mm (this study).
30	Soft	Soft fouling (eg filaments) <76 mm in length and <6.4 mm in height.
40	Hard	Tubeworms <6.4 mm in height. Encrusting bryozoans (this study).
50	Hard	Barnacles <6.4 mm in height.
60	Hard	Combination of tubeworms and barnacles <6.4 mm in height.
70	Hard	Combination of tubeworms and barnacles > 6.4 mm in height.
80	Hard	Tubeworms closely packed and upright from surface, or barnacles on top of each other, < 6.4 mm in height.
90	Hard	Densely packed tubeworms or barnacles, > 6.4 mm in height; presence of mussels or oysters; or slime/grass overlay.
100	Composite	All forms of fouling; soft animal fouling (tunicates) growing on various forms of hard fouling

determined for the immersion time $t = 364$ days, where E_i corresponds to the initial DFT upon deployment, and E_t corresponds to the DFT at immersion time t. Measurements were only taken on cleaned panels, to avoid biofouling thickness as a confounding effect. The equivalent total biocide loss was then determined by multiplying $E_i - E_t$, in μm, by the active substance loading, or ASL:

$$ASL \left[\frac{\text{μg biocide}}{\text{μm cm}^2} \right] = \frac{Paint\ density\ \left[\frac{\text{g}}{\text{cm}^3} \right] \times Wet\ weight\ fraction\ [\%]}{Volume\ of\ solids\ fraction\ [\%]} \times \frac{10^6\ [\text{μg/g}]}{10^4\ [(\text{μm cm}^2)/\text{cm}^3]}$$

(5)

where, for the current coating PPG Sigma Ecofleet® 290 (AF panels), nominal wet paint density was 1.7 g cm^{-3}, nominal wet weight fraction was up to 50% for copper (I) oxide and up to 10% for zineb, and volume of solids fraction was $55 \pm 2\%$, according to product documentation (Sigma Färg, Mölndal, Sweden). Unfortunately, uncertainties on nominal values for biocide wet weight fraction and wet paint density were not available from the manufacturer. For AF panels, Equation 5 yields an ASL of ≤ 155 μg Cu$_2$O μm^{-1} cm^{-2} (or ≤ 137 μg Cu μm^{-1} cm^{-2}), and ≤ 30.9 μg zineb μm^{-1} cm^{-2}.

Leached layer thickness

After each cleaning event, AF coated panels might still present a leached layer, where biocide content is lower than on deeper layers of intact coating (Kiil and Yebra 2009). The existence of a leached layer would mean that the biocide release rate is underestimated using the polishing rate mass-balance method. This underestimation would arise from the amount of biocide released from the top layer of the coating, i.e. the leached layer, which is not associated with any measurable change in total paint thickness (Howell and Behrends 2006). In agreement with such underestimation, Tribou and Swain (2017) had already noted that the polishing rate mass-balance only represents stabilized release rates, whereas other methods such as chemical analysis of leachates enable to detect peaks in release rate (Tribou and Swain 2017).

To evaluate the extent to which the polishing-rate mass-balance method underestimates the biocide release rate, leached layer thickness was currently determined using Scanning Electron Microscopy (SEM) coupled with Energy Dispersive X-ray (EDX), for imaging and chemical analysis of cross-sections of panels coated with AF. A newly-applied coating, as well as immersed non-cleaned (AFS0F0) and cleaned

AF panels (AFS1F1, AFS1F2), were sampled in triplicate. Sample preparation and imaging procedures followed those presented in Howell and Behrends (2006), with some modifications: (1) the last polishing step for obtaining cross-sections of the coating was done with a wetted P4000 carbide paper on the polishing wheel, instead of a 6-μm diamond polishing solution, (2) a lower acceleration voltage was used, corresponding to 20 kV instead of 25 kV, which was high enough for back-scatter electron imaging and EDX analysis; (3) for more comprehensive EDX analysis, instead of single line scans along depth, profiles were averaged from a total of 30 line scans, spaced by 3-μm steps along the coating surface and with a 0.5-μm resolution along coating depth.

Paint damage and roughness

Panels were visually inspected for different types of paint damage. Additionally, peak-to-valley roughness height ($R_{t,50}$) was also determined on both newly-applied and cleaned coatings.

For paint damage inspection, different types of damage were defined following the standard test method ASTM D6990-05. Extent diagrams were used for estimating percentage cover, as given in that same standard (ASTM D6990-05. 05 2005). Any damage occurring within a 3-cm margin around each half panel was discounted for possible edge effects.

Paint condition was also evaluated using the peak-to-valley roughness height at 50-mm cut-off length, i.e. MHR (Mean Hull Roughness). This definition of roughness height is conventionally used for estimating penalties on ship hydrodynamic resistance that are associated with bare paint roughness, using Townsin's formula (ITTC 2014). Presently, peak-to-valley roughness was determined using the TQC Hull Roughness Gauge DC9000 (TQC B.V., Capelle aan de IJssel, the Netherlands). This instrument has an accuracy ± 5 μm or ± 2% of the actual reading, whichever is greater. Measurements were taken on two occasions: (1) before deployment, and (2) at the end of the study, after indoors drying of cleaned panels for more than seven days. Three repeated measurements were taken along the cleaning path of the waterjet (Figure 1), i.e. three repeats per half panel, yielding one value of MHR per panel replicate. For the foul-release coating (FR: PPG Sigmaglide® 1290), peak-to-valley roughness was measured under wet conditions to avoid the stylus probe from juddering over the dry rubbery surface of the coating. The surface was thus moisturized prior to measurement, using a handheld

water spray, as per recommendation from the probe manufacturer (Townsin 2012).

Statistical analysis

With the exception of anti-corrosive epoxy (E) coated panels, which were deployed as single panels for evaluating fouling pressure on a monthly basis (Table 2), three replicate panels were included under each treatment. For determining whether the top coating, cleaning frequency or nozzle translation speed had any significant effect on the results, non-parametric analysis of variance was performed using the Kruskal-Wallis test (MATLAB® version R2017b, MathWorks, Natick, MA, USA). Additionally, 95% confidence intervals (CI-95) were determined, by multiplying the standard error by the two-tailed t-value with $n - 1$ degrees of freedom, where n is the number of observations (Montgomery 2013).

Results and discussion

Non-cleaned panels

In Figure 3, areal-mean fouling rating is plotted, as calculated from Equation 3. Monthly fouling pressure at the site, from anti-corrosive epoxy E panels, varied between an areal $mean(fr_{NSTM})$ ~10 in the winter months November – April (Figure 3a, EPS0F0, $t = 1$ month and $t = 8$ to 12 months), reaching peak values of $mean(fr_{NSTM})$ of 70 to 90 in the summer months of June and September 2018 (Figure 3a, EPS0F0, $t = 3$ and 6 months). These values set the range for areal-averaged monthly fouling pressure between an incipient slime in the winter (Figure 4a), and hard fouling covered with macroalga in summer months (Figure 4b). Incipient slime ($fr_{NSTM} = 10$) is distinguished from advanced slime ($fr_{NSTM} = 20$) based on whether the underlying coating is discernible (incipient slime) or obscured by microfouling (advanced slime, Table 3). Individuals are discernible by naked eye starting at an fr_{NSTM} of 30 (soft filamentous macrofouling, e.g. macroalgae).

Panels coated with fouling-control coatings that were never subjected to any cleaning, i.e. AFS0F0 and FRS0F0, were observed to foul progressively from an areal $mean(fr_{NSTM}) \sim 0$ after the first month (Figure 3a, $t = 1$ month) to a final $mean(fr_{NSTM}) = 20\text{-}40$ (Figure 3a, $t = 12$ months). Representative photographs of these non-cleaned AF and FR panels are given in Figure 4c and Figure 4e, respectively, in their final condition. Significant differences between biocidal coating AF and FR are noted on nearly half of

the occasions, on which non-biocidal FR panels were less fouled than AF (Figure 3a, $t = 3$, 5, 8, 9 and 11 months). Also, from time-averaged $\overline{mean(fr_{NSTM})}$ values in Figure 5, which were calculated from areal mean values using Equation 4, non-cleaned FR panels (FRS0F0) had a significantly lower fouling rating, with time-averaged $\overline{mean(fr_{NSTM})}$ significantly below 10 (incipient slime), than non-cleaned AF panels (AFS0F0), with $\overline{mean(fr_{NSTM})}$ significantly above 10 (Figure 5a). The lower fouling rating on FR panels could be due to local currents keeping these panels relatively clean. Thus, even though velocity magnitudes near the panels, as sampled with ADV (please refer to Field test site, under Materials and methods), were below 0.30 m s^{-1} (~0.6 knots), wave and propeller action from passing boats and extreme weather events, such as not sampled with the ADV, might help explain the significant drop in areal mean fr_{NSTM} for FR panels observed on $t = 8$ months (Figure 3a). For example, a severe gale was experienced during one night on 28-29 November 2018, with 7 h of hourly wind speed > 20 m s^{-1} (SMHI. 2019). Finally, the initial mechanical action of silicone oils on FR panels should not be overlooked, considering that during the first three months from deployment a thin film of oil could be observed on the sea surface on retrieving the panels for monthly inspections. Such silicon oils were previously reported as mechanically interfering with barnacle larvae, by immobilizing them (Watermann et al. 2005).

Cleaned panels

Fouling ratings on panels cleaned at bi-monthly or monthly frequencies are plotted in Figure 3b and Figure 3c, respectively, which follow saw-shaped functions. Representative photographs of the after-cleaning condition are shown in Figure 4d and Figure 4f, respectively for AF and FR coated panels, where cleaning paths can be clearly identified, following the expected pattern of Figure 1.

In the areal mean fr_{NSTM} plots of Figure 3b-c, it is observed that, within the interval between cleanings (bi-monthly, F1, or monthly, F2), fouling quickly grew back to levels close to non-cleaned panels (Figure 3a). This seems to suggest that a higher cleaning frequency would be required in order to significantly decrease fouling rating, namely bi-weekly or even weekly cleanings. However, by calculating time-averaged values for different treatments, some decrease in time-averaged $\overline{mean(fr_{NSTM})}$ is noted with increasing cleaning frequency (Figure 5a), where a significant drop in time-
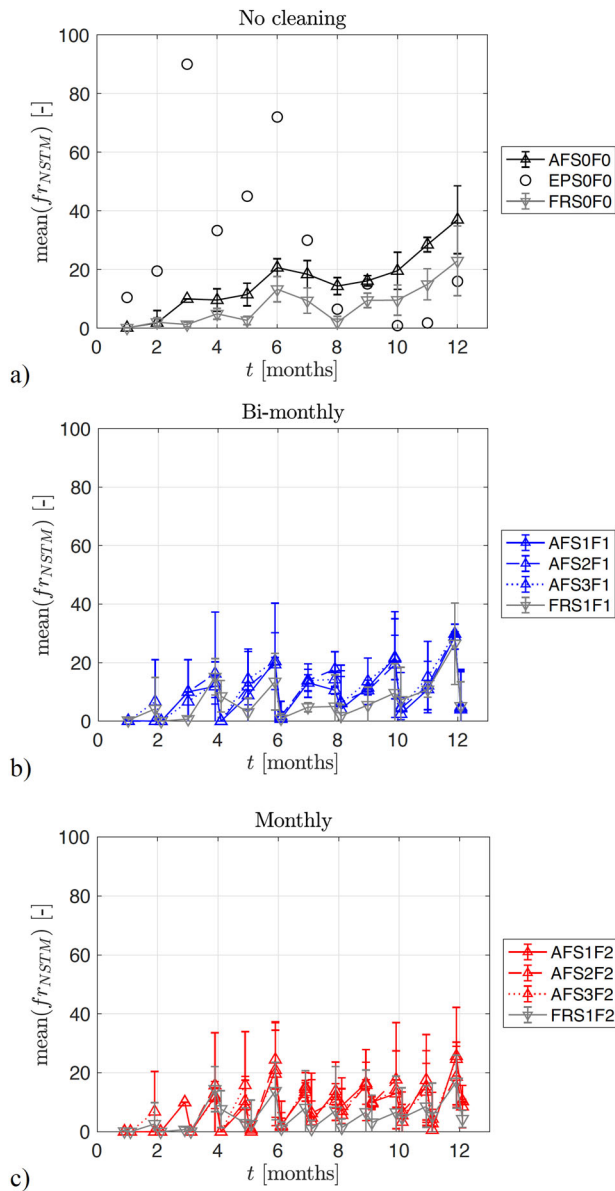
a)

Figure 3. Areal-mean fouling rating *vs* time, for different coatings (AF, E, FR) and cleaning frequencies: (a) no cleaning, F0; (b) bi-monthly cleanings, F1; (c) monthly cleanings, F2. For E panels, plotted values correspond to the final stage after each period of one-month exposure, corresponding to 12 different panels deployed and retrieved on a monthly basis. For AF panels, the nozzle translation speed was varied (S1: 0.01 m s^{-1}; S2: 0.02 m s^{-1}; S3: 0.03 m s^{-1}).

Figure 4. Representative examples of fouling rating: (a) E panel (March 2019, $t = 11$ months): $fr_{NSTM} = 10$ (15%), $fr_{NSTM} = 30$ (1%); (b) E panel (October 2018, $t = 6$ months): $fr_{NSTM} = 30$ (20-40%), $fr_{NSTM} = 90$ (60-80%); (c) non-cleaned AF panel (April 2019, $t = 12$ months): $fr_{NSTM} = 30$ (100%); (d) cleaned AF panel (April 2019, $t = 12$ months): $fr_{NSTM} = 10$ (3-99%), $fr_{NSTM} = 20$ (0-1%); (e) non-cleaned FR panel (April 2019, $t = 12$ months): $fr_{NSTM} = 10$ (30-40%), $fr_{NSTM} = 20$ (0-30%), $fr_{NSTM} = 30$ (0-50%), $fr_{NSTM} = 90$ (5-40%); (f) cleaned FR panel (April 2019, $t = 12$ months): $fr_{NSTM} = 10$ (30-60%).

averaged fouling rating is detected from non-cleaned AF, AFS0F0 with $\overline{mean(fr_{NSTM})}$ significantly above 10 (incipient slime), to bi-monthly cleaned AF, AFS1F1 with $\overline{mean(fr_{NSTM})}$ significantly below 10 (propagated 95% confidence intervals). Although this behaviour is expected to differ for an active vessel, with lower growth rate on an intermittently moving hull compared to non-cleaned AFS0F0, the pattern observed on static panels might still be relevant for niche areas
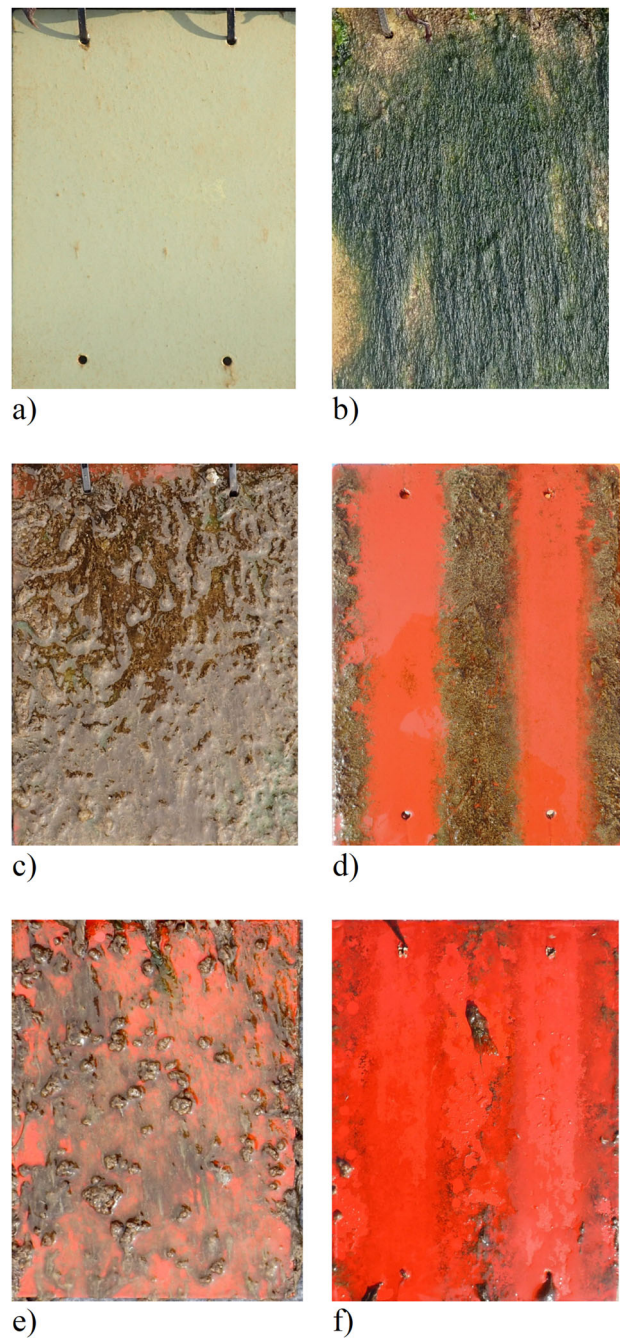
sheltered from hydrodynamic forces, namely recesses on the hull and sea chests. Finally, no significant decrease is detected for the corresponding cases on FR panels, i.e. no significant drop from FRS0F0 to FRS1F1
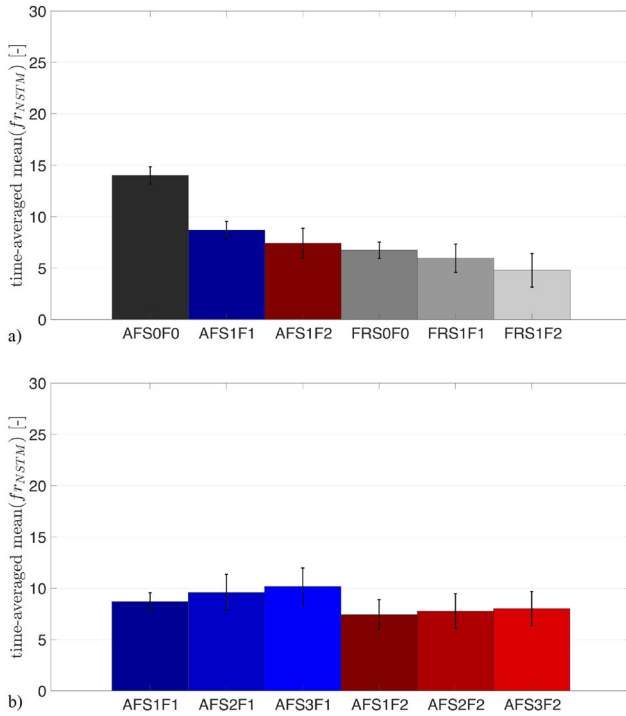
Figure 5. Time-averaged fouling rating, calculated from areal-mean fouling rating along time using the trapezoidal rule (Equation 4), where error bars correspond to propagated 95% confidence intervals: (a) AF and FR panels, with either no cleaning or constant translation speed (S0 for no cleaning; S1 for 0.01 m s^{-1}) and varying cleaning frequency (F0 – no cleaning, F1 – bi-monthly, F2 – monthly); (b) AF panels, with varying translation speed (S1: 0.01 m s^{-1}; S2: 0.02 m s^{-1}; S3: 0.03 m s^{-1}).

Figure 6. Adhesion strength, or local cleaning areal forces (in Pa), used in different points in time, depending on cleaning results, for two fouling control coatings (AF and FR), three cleaning frequencies (F0 – no cleaning; F1 – bi-monthly cleanings; F2 – monthly cleanings) and three nozzle translation speeds (S1: 0.01 m s^{-1}; S2: 0.02 m s^{-1}; S3: 0.03 m s^{-1}): (a) maximum wall shear stress $\tau_{w,max}$; (b) stagnation pressure p_s. Error bars correspond to 95% confidence intervals.

(Figure 5a), due to the already low level of fouling, with a time-averaged $\overline{mean(fr_{NSTM})}$ already well below 10 for non-cleaned panels, FRS0F0.

Interestingly, after the first few months, the fouling rating after each cleaning event did not always drop to a null $mean(fr_{NSTM})$ (Figure 3b-c). These non-zero values correspond to reaching the maximum design cleaning forces of the current waterjet setup, which were ~0.5 kPa and ~0.07 MPa for maximum shear stress and stagnation pressure, respectively, with standoff distance $H = 25$ mm, as plotted in Figure 6a-b for $t < 10$ months. The occurrence of non-zero fouling ratings after cleaning is associated with development of tenacious biofilms on both AF and FR coatings, as observed on Figure 4d and Figure 4f, respectively, which were also reported in previous studies in warmer waters (Hearin et al. 2015, 2016; Hunsucker et al. 2018). Tenacious biofilms differ from regular biofilms by their low-form profile (i.e. low wet film thickness) and ability to withstand grooming forces (Hearin et al. 2016). Tenacious biofilms are presently defined as those withstanding the maxi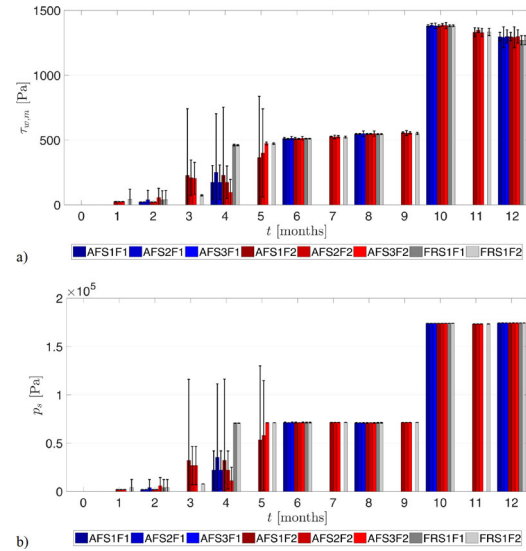mum force applied by the waterjet setup. The FR coating developed a visible tenacious biofilm from the fourth month onwards, whereas on AF panels this biofilm was detected from the fifth month onwards (Figure 3b-c). Comparable periods have been reported in the literature, where tenacity was detected within one to three months in grooming tests conducted on FR and AF coatings, respectively (Hearin et al. 2015, 2016). Along with adhesion-strength testing on FR coatings, Hunsucker (formerly Zargiel) and Swain studied the composition of microfouling communities on such coatings, and could associate tenacity against removal to species composition (Zargiel and Swain 2014; Hunsucker and Swain 2016).

In an attempt to remove tenacious biofilms, a lower standoff distance $H = 16$ mm was used for $t \geq 10$ months, enabling higher local wall shear stress up to ~1.3 kPa and stagnation pressure up to ~0.17 MPa on the last three monthly-cleaning events (Figure 6a-b, $t \geq 10$ months). However, this increase in cleaning forces had a negligible effect on the tenacious biofilms, which were still observed after cleaning (Figure 3b-c, $t \geq 10$ months). As these biofilms are typically removable by touch (Hearin et al. 2016), considerably higher cleaning forces should have been selected from the start, thus possibly reducing the biomass of tenacious biofilms. However, this approach would come with increasing the risk of damage and wear to the coating, and stronger selection for even more tenacious biofilms.

Barnacle counting for different treatments (Table 4) reveals that current cleaning forces enabled removal of adult barnacles from FR panels, since no barnacles could be observed after any of the cleaning events (Table 4). Also, non-cleaned FR panels were mostly free of barnacles during the summer, except for limited barnacle settlement in July 2018 (Table 4). Such limited barnacle fouling on non-cleaned FR panels might have been subsequently predated on, or else removed by local currents, since those barnacles (Table 4, non-cleaned FR panels, July 2018) were not detected from August 2018 onwards. Again, low barnacle fouling during the summer on FR panels is currently attributed to mechanical action of the silicone oil on barnacle larvae (Watermann et al. 2005). Subsequently, FR panel performance deteriorated from January 2019 onwards, with significant counting of adult barnacles on non-cleaned FR panels (Table 4), which is most probably due to depletion of surface oil (Yebra et al. 2004). No barnacles developed into the adult stage on AF panels, and for this reason these panels are excluded from Table 4. Finally, cleaning frequency would probably need to be increased in geographical regions of higher fouling pressure, e.g. up to weekly maintenance events (Hunsucker et al. 2018), in order to insure a comparable coating performance under idle conditions. Also, the effectiveness of the waterjet is currently unknown for fouling ratings higher than presently observed.

In Figure 5b, time-averaged fouling ratings for varying nozzle translation speed are compared (AF panels only). The aim here was to determine whether translation speed had any significant effect on coating performance, which is relevant since hull cleaning is conducted within a limited time frame. Differences between treatments are within confidence intervals, though there seems to be ∼8-17% increase in time-averaged fouling rating with increasing translation speed (Figure 5b: from $mean(fr_{NSTM})$ ∼8.7 to ∼10.2,

for bi-monthly cleanings, or from ∼7.4 to ∼8.0, for monthly cleanings). Such increase in fouling rating would be in agreement with a time-dependent result from cleaning, where cleaning is more effective at lower translation speed. However, in the studied range of translation speed, differences are not statistically significant.

Adhesion strength values were obtained for the current AF and FR coatings (Figure 6), with maximum shear stress and stagnation pressure within 0.5 kPa and 0.07 MPa bringing down areal mean fr_{NSTM} to zero within the first three months from deployment (Figure 3b-c). From the fifth month onwards, tenacious biofilms were observed on both AF and FR coatings. Later on, by the tenth month, increasing the maximum shear stress and stagnation pressure to ∼1.3 kPa and ∼0.17 MPa (respectively) did not enable removal of tenacious biofilms. Thus, it is recommended that the current adhesion strength values be referred to as the lower boundary for forces required to keep these coatings at $mean(fr_{NSTM})$ of ∼10 (incipient slime), bearing in mind that corrections for time-dependency of cleaning results should be applied for fast-translating nozzles, e.g. as used in full scale cleaning devices. However, in order to scale adhesion strength results for a faster cleaning device, i.e. working at higher translation and rotation speed, the current high uncertainties in adhesion strength do not enable establishing a robust relationship between required cleaning forces, i.e. $\tau_{w,max}$ or p_s, and translation speed, S1-S3 (Figure 6). Uncertainties in Figure 6, namely the wider confidence intervals during months three through five, arise from a combination of low number of flowrate steps (Table 1: only four steps applied from the third cleaning event onwards), a modest number of replicate panels (triplicates), and a considerable degree of subjectivity implied in determining that a surface is visually clean ($fr_{NSTM} = 0$).

Table 4. Barnacle counting on epoxy anti-corrosive (E) and foul-release (FR) coated panels, individuals dm^{-2} (mean ± 95% confidence interval), before/after each cleaning event.

Month	E (1 panel per month)	FR: no cleaning (F0)	FR: bi-monthly (F1)		FR: monthly (F2)	
			Before	After	Before	After
2018 May	0	0	0		0	0
2018 Jun	0	0	0	0	0	0
2018 Jul	+	+	0		0	0
2018 Aug	85	0	2 ± 7	0	1 ± 5	0
2018 Sept	+	0	0		0	0
2018 Oct	+	0	0	0	0	0
2018 Nov	0	0	0		0	0
2018 Dec	4	0	0	0	0	0
2019 Jan	567	19 ± 10	10 ± 24		9 ± 20	0
2019 Feb	0	58 ± 28	11 ± 4	0	0	0
2019 Mar	0	52 ± 13	0		0	0
2019 Apr	0	16 ± 17	0	0	0	0

(+) adult barnacles detected but no counting available for that date.

For example, in Figure 6 – month three, AFS1F2 required flowrates for achieving a visually-clean surface on triplicate panels in a range as wide as 1.0-3.0 l min^{-1} (see Supplemental materials), or wall shear forces in the range ~80-530 Pa (Table 1). In order to exclude any issues with subjective judgement on visually-clean surfaces, future studies would benefit from using a suitable, non-destructive method for detecting and quantifying thin biofilms, such as quantitative fluorescence-based methods (Fischer et al. 2014). Also, a suitable threshold for a 'clean surface' should then be applied throughout, e.g. based on instrument detection limit.

Polishing rate and biocide release rate

Biocide release rate was studied on cleaned AF panels, using the polishing rate mass-balance method, which relies on changes in paint thickness for calculating the amount of released biocide. This method was complemented with SEM-EDX imaging and chemical analysis for determining the extent of underestimation due to formation of a leached layer on the AF coating (Howell and Behrends 2006; Kiil and Yebra 2009).

In Figure 7, the amount of polishing $E_i - E_t$ is plotted for different cleaning treatments, with varying nozzle translation speed and cleaning frequency. Total polishing was ~30-35 μm by the end of one-year's immersion, and no significant differences were observed between treatments (Kruskal-Wallis test, $p = 0.6$). Thus, current observations appear to indicate there is no evidence of increased polishing due to cleaning events. However, tenacious biofilms were present on the coating at the end of the study, and these may have affected the polishing rate results. Considering that at the end of the study bi-monthly

cleaned panels had, on average, half the areal mean fouling rating, with $mean(fr_{NSTM})$ ~5, compared to monthly-cleaned panels, with $mean(fr_{NSTM})$ ~10 (see raw data in Supplementary materials), this may have had an impact on the results, leading to underestimation of the difference in wear between cleaning frequencies. To the best of the authors' knowledge, this is the first account where fouling is raised as a confounding factor in DFT measurements (there is no mention to this issue in Haslbeck and Ellor 2005, Finnie 2006, or Tribou and Swain 2017). Tribou and Swain (2017) inclusively conducted DFT measurements on ungroomed panels, without mentioning fouling as a potential confounding factor.

By applying the nominal active substance loading of the current coating, i.e. $ASL = 137$ μg Cu μm^{-1} cm^{-2} (Equation 5), and an immersion time of $t = 364$ days, an average copper release rate of ~13 μg Cu cm^{-2} day^{-1} is estimated (Figure 7). This release rate is of the same order of magnitude as previously reported values obtained using the same method on erodible coatings: for in-service conditions on US Navy vessels, values ranging 7.6-18 μg Cu cm^{-2} day^{-1} were reported (Haslbeck and Ellor 2005), and values as high as 21.1 and 28.1 μg Cu cm^{-2} day^{-1}, respectively for monthly- and weekly-groomed panels (Tribou and Swain 2015). However, it should be noted that the AF products used differ between studies, as well as environmental conditions, it being known that temperature, pH and salinity may significantly impact biocide release rates (Sanchez and Yebra 2009; Lagerström et al. 2018). Also, grooming forces applied at the coating level are unknown in the study by Tribou and Swain (2015). Therefore, absolute comparisons are currently limited to a plausibility check on the order of magnitude.
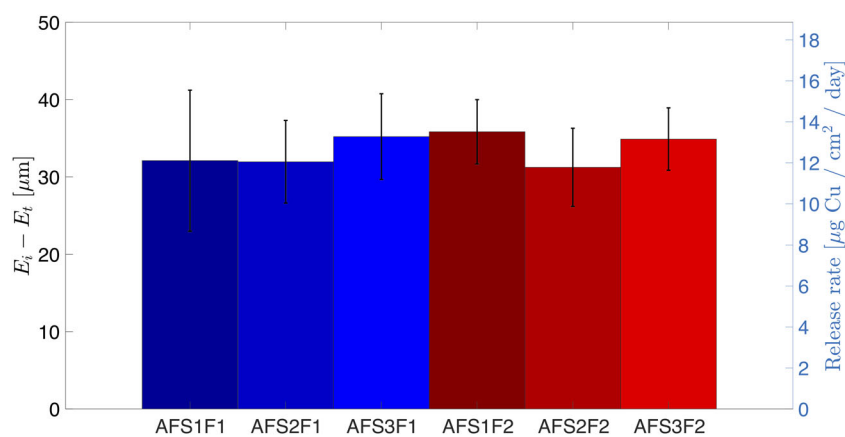

Figure 7. Paint polishing $E_i - E_t$ for each treatment, together with corresponding copper release rate (Kruskal-Wallis test: $p = 0.6$). Error bars correspond to 95% confidence intervals.

After each cleaning event, AF panels might still present a leached layer, where biocide content is lower than in deeper layers of intact coating (Yebra et al. 2004), which leads to an underestimation in the above polishing-rate method. The thickness of the leached layer was currently determined using SEM-EDX. Due to time constraints, EDX profiling was only performed on immersed non-cleaned (AFS0F0) and monthly-cleaned AF samples (AFS1F2). Imaging of a newly-applied coating revealed metal grains all the way up to the surface (Figure 8a, left-hand side), as expected for an intact coating, i.e. before immersion and leaching. For immersed coatings (Figure 8b-d), a top layer was detected, where the metal grains fade out near the surface, this being identified as the leached layer. From EDX analysis, counts for each metal element relative to the intact coating were determined along depth (Figures 8b and 8d), enabling better determination of the extent of the leached layer. From these profiles, the leached layer spaned $\sim$20-30 μm, measured from the insoluble iron pigment front (Fe), within which there was a gradual increase in both Cu and Zn counts. Surprisingly, cleaning with the waterjet did not lead to removal of the leached layer, as there were no observed differences between non-cleaned (Figure 8b) and cleaned samples (Figure 8c and 8d). Thus, considering that the last cleaning event did not erode the leached layer, the equivalent biocide loss given in Figure 7 is underestimated by at least the amount of biocide released from the remaining leached layer, which is of the same order of magnitude as the amount determined from polishing.

Taking into consideration possible errors introduced by tenacious biofilms and leached layers, the above polishing rate mass-balance results should be interpreted with caution. For the current purpose of comparing cleaning treatments, i.e. as a function of cleaning frequency and nozzle translation speed, and considering approximate agreement between leached layers developed on immersed samples (Figure 8b–8d), the underestimation due to leached layers seems to be approximately constant across all treatments. However, unknown errors associated with tenacious biofilms developing differently for different treatments require further investigation, e.g. using cross-validation with other methods for determining biocide release rates, using chemical analysis of leachates and coatings (Finnie 2006; Lagerström et al. 2018).

Finally, even though no significant wear could be currently attributed to monthly/bi-monthly cleaning events, which supports the use of minimal removal forces matching the adhesion strength of fouling, the above testing should be extended to periods of 2-5 years, i.e. the typical dry-docking interval for large commercial vessels, in order to test for long-term effects of such maintenance practices.

Paint damage and roughness

Paint damage was evaluated according to definitions in the standard test method ASTM D6990-05, and using extent diagrams given in the same standard (ASTM D6990-05. 05 2005). Additionally, peak-to-valley paint roughness was measured on panels before deployment, and also after the final cleaning event (dried panels).

Only three types of damage, all to a minor extent, could be detected in this study (Supplemental materials), and these corresponded to chipping on AF coated panels, only detected during the first three months, localized corrosion pitting on AF panels, and localized damage (scratches) on cleaned AF and FR coated panels. However, any type of damage was invariably detected at low percentage cover, $\leq$1%. These observations support the claim that cleaning at adhesion-strength level does not result in significant damage to the coatings.

Peak-to-valley roughness height was measured on both fouling-control coatings (AF and FR panels), before immersion ($t = 0$) and at the end of the study, for panels that were waterjet cleaned ($t = 12$ months). The results are presented in Figure 9, and show a significant initial difference between coatings ($t = 0$ months, Kruskal-Wallis test: $p = 0.0010$), which remains significant at the end of the study ($t = 12$ months, Kruskal-Wallis test: $p = 0.0014$) where the FR coating, with MHR $\sim$70 μm (PPG Sigmaglide® 1290), was significantly smoother than the AF coating, with MHR $\sim$90-110 μm (PPG Sigma Ecofleet® 290). These differences in roughness height are primarily attributed to varying paint formulation and the quality of paint application, since paints were applied at different painting facilities (AB Gotenius Varv, Gothenburg, and PPG Research Center Amsterdam, the Netherlands). Finally, no increase in roughness height could be detected as a result of the cleaning. Indeed, the AF coating (PPG Sigma Ecofleet® 290) got significantly smoother by the end of the study, dropping from $\sim$110 to $\sim$90 μm peak-to-valley roughness height. However, this may not solely be attributed to the effect of cleaning, but also to the self-smoothing effect, typical of some AF self-polishing coatings (Yebra et al. 2004).

Overall, above results for the AF coating (polishing rate, leached layer, paint damage, and paint roughness) indicate that cleaning had no detectable effect
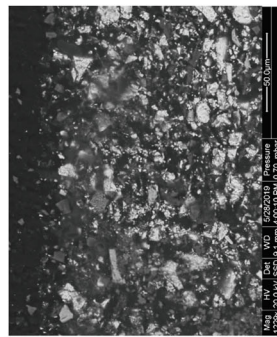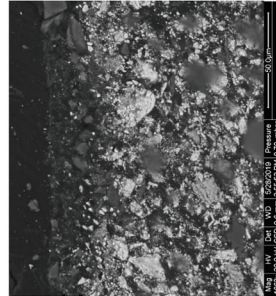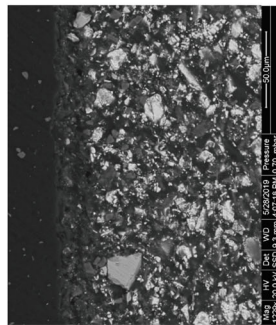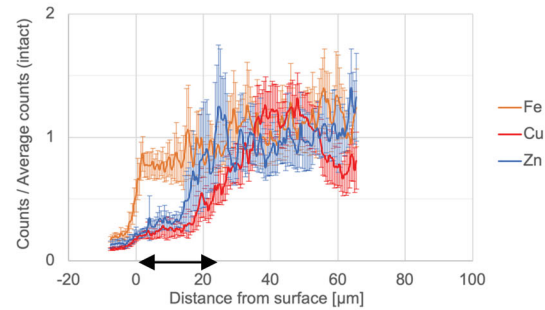
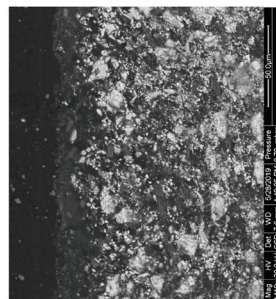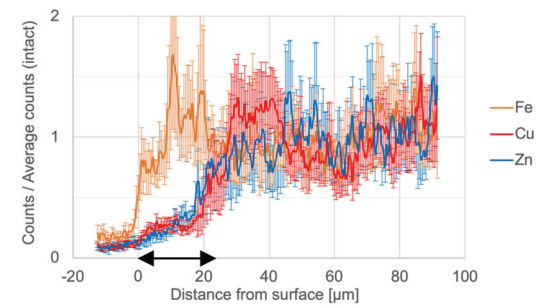Figure 8. SEM imaging of coating cross-sections (AF), where the surface of the coating is on the left-hand side (approximate leached layer thickness is marked by double arrows), together with element-count profiles along depth, from EDX analysis: (a) newly applied; (b) immersed non-cleaned – AFS0F0; (c) immersed and cleaned bi-monthly – AFS1F1); (d) immersed and cleaned monthly – AFS1F2. Element abundance is expressed as a ratio between EDX counts and average counts on deeper, intact layers of the coating. Scale bars (upper right corner on SEM images) correspond to 50 μm, and error bars correspond to 95% confidence intervals for 30 line scans.
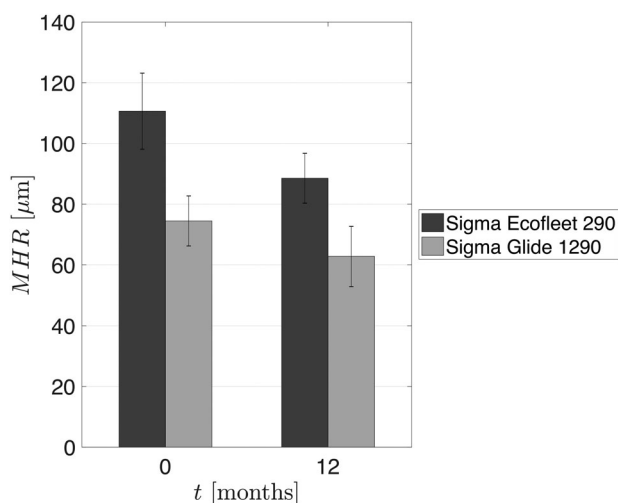
Figure 9. Peak-to-valley roughness height, *MHR* (Mean Hull Roughness), for anti-fouling paint PPG Sigma Ecofleet® 290 (AF panels) and foul-release PPG Sigmaglide® 1290 (FR panels), before or after immersion and waterjet cleaning (Kruskal-Wallis test: $p = 0.0010$ and 0.0014, at $t = 0$ and 12 months, respectively). Error bars correspond to 95% confidence intervals for n cleaned panels under each coating, i.e. $n = 18$ AF panels (triplicates of six cleaning treatments were pooled) and $n = 6$ FR panels (triplicates of three cleaning treatments were pooled).

on coating condition, while being effective at reducing the level of fouling (Figure 5a).

Implications for shipowners and hull cleaning practitioners

From a shipowner/operator perspective, it might be uneconomical to run a ship with the level of fouling reported here for unprotected epoxy (E) panels, on which areal $mean(fr_{NSTM})$ scored as high as 70-90 (hard fouling). For such levels of fouling, and depending on vessel type and speed, penalties in propulsive power could easily reach 40-130% for keeping the same vessel speed (Schultz 2007; Demirel et al. 2017). Thus, in order to minimize fuel costs and emissions to the atmosphere, it is clear that a suitable fouling-control coating is required, potentially in combination with in-water cleaning or hull grooming.

Considering the performance of fouling control coatings, i.e. AF panels or FR panels deployed under local almost-static flow conditions near the Port of Gothenburg (Figure 5), and comparing cleaned panels to non-cleaned panels, some improvement in terms of lower fouling rating could be achieved by increasing cleaning frequency. However, such improvements were within the lowest fouling rating $fr_{NSTM} = 10$, i.e. incipient slime, and were not statistically significant, except for non-cleaned AF panels, which scored

significantly above a time-averaged $\overline{mean(fr_{NSTM})}$ of 10 (Figure 5a). Also, the available calculations on the effects of fouling on propulsive power have, at least for the time being, limited resolution in this lower range of slime fouling (Schultz 2007; Murphy et al. 2018). Nevertheless, it can be hypothesized that increasing cleaning frequency to weekly or bi-weekly would probably enable a stable areal-mean fouling rating of $mean(fr_{NSTM})$ ∼10 to be retained, compared to a final observed fouling rating of $mean(fr_{NSTM})$ ∼ 40 for non-cleaned AF panels (Figure 3a). These levels of fouling would correspond roughly to propulsive power penalties of 10-20% in the first case, compared to 30-60% increase in power in the second case, again depending on vessel type and speed (Schultz 2007; Demirel et al. 2017). Since surfaces covered in slime can be highly variable in terms of texture, roughness height and mechanical properties (Murphy et al. 2018), any comparison in terms of propulsive penalties in this range of fr_{NSTM} is subject to high uncertainty, and further hydrodynamic characterization would be required in terms of drag properties of the particular surfaces discussed in this paper. Additionally, it should be stressed that active vessels are expected to have a lower level of fouling and growth rates compared to those reported here. Therefore, cleaning frequencies recommended here, namely more frequent than monthly, might not be optimal for specific vessels, depending on their operational speed profile. Finally, even though slime and algae may constitute a significant portion of in-service fouling (Swain and Lund 2016), the tenacity of micro-fouling might be higher on the main areas of the hull, compared to niche areas that are less exposed to hydrodynamic stress (e.g. hull recesses, sea chests and box coolers). Thus, further adhesion testing on dynamically exposed coatings will be required in order to determine the adhesion properties and cleaning frequencies for hull surfaces exposed to similar hydrodynamic conditions as experienced on main areas of active hulls (e.g. ASTM D4939–8989 2003; Lindholdt, Dam-Johansen, Yebra et al. 2015).

Considering the current findings and the ephemeral properties of slimed surfaces, developers and operators of hull cleaning devices are advised to test the efficacy of their devices on a limited but representative fouled area of the hull, and from there, select cleaning parameters. Currently reported values of adhesion strength may provide a guide on minimal cleaning forces, while also taking into consideration the treatment time, as set by nozzle translation and rotation speeds.

Conclusions

In spite of significant development in fouling-control of ship hull coatings, in-water hull cleaning is still performed on commercial vessels. The current study used an immersed waterjet setup for testing quantified wall forces on different fouling-control coatings. Coatings were immersed under local almost-static flow conditions on the west coast of Sweden, and cleaned at varying frequency and nozzle translation speed.

By applying minimal cleaning forces on an AF biocidal coating panels and biocide-free FR panels, no significant wear or damage was reported (one-year study), though further improvement is deemed necessary in terms of accuracy in biocide release estimates for future use in environmental risk assessment. The amount of fouling (fouling rating) could be lowered to some extent by bi-monthly or monthly cleaning, with a significant decrease in fouling rating for the biocidal coating. However, for active vessels, the need for cleaning would be admittedly lower, except for niche areas on the hull that are sheltered from hydrodynamic forces, e.g. hull recesses and sea chests. Finally, the highest tested cleaning forces, i.e. wall shear stress of $\sim$1.3 kPa and stagnation pressure $\sim$0.17 MPa, were still unable to remove tenacious biofilms that formed on both AF and FR coatings (nozzle translation speed: 0.01-0.03 m s^{-1}).

The current results may be used in improving the design and operation of cleaning devices, which should aim at matching the adhesion strength of microfouling. Future research is required on the long-term validity of these results in 2- to 5-year studies, and also on translating current results into full-scale cleaning parameters. Specifically, forces applied by different full-scale devices need to be determined, while acknowledging possible time-dependencies of both the cleaning results and damage/wear to hull coatings.

Nomenclature

ASL	active substance loading
D	nozzle inner diameter
$E_i - E_t$	paint polishing, in dry film thickness
fr_{NSTM}	fouling rating according to the US Navy Technical Ship Manual (2006)
H	jet standoff distance
n	number of observations
N	number of visible fouling ratings on a surface
p_s	stagnation pressure
Q	nozzle flowrate
r	radial distance from jet impingement
Re_D	Reynolds number based on nozzle diameter, $Re_D = u_0 D/\nu$
MHR	Mean Hull Roughness, ie peak-to-valley roughness height at cut-off length 50 mm
t	elapsed time since deployment
u_0	mean velocity through nozzle, $u_0 = 4Q/(\pi D^2)$
u_t	nozzle translation speed
x, y, z	coordinates for nozzle translation, alignment and standoff, respectively
ν	kinematic viscosity of the fluid
ρ	density of the fluid
$\tau_{w,max}$	maximum wall shear stress at the wall

Abbreviations

ADV	Acoustic Doppler Velocimeter
AF	anti-fouling coating
CI-95	95% confidence intervals
DFT	dry film thickness
E	epoxy anti-corrosive coating
F	cleaning frequency
FR	foul-release coating
ROV	remotely operated vehicle
S	nozzle translation speed
SD	standard deviation
TBT	tributyl tin

Supplemental materials

Sensitivity analysis for surface forces under an immersed vertical jet (six figures) Spreadsheet 1/2: *Paint_damage_accor ding_to_ASTM_D6990-05.xlsx* Spreadsheet 2/2: *Raw_data.xlsx*

Acknowledgements

Disclosure statement

No potential conflict of interest was reported by the author(s).

Funding

ORCID

Dinis Reis Oliveira http://orcid.org/0000-0001-8948-6884
Lena Granhag http://orcid.org/0000-0002-0340-7469

References

ASTM D4939–89. 2003. Standard test method for subjecting marine antifouling coating to biofouling and fluid shear forces in natural seawater (Reapproved 2003). West Conshohocken, PA.

ASTM D5618. 1994. Measurement of barnacle adhesion strength in shear (Reapproved 2011). West Conshohocken, PA.

ASTM D6990-05. 2005. Standard practice for evaluating biofouling resistance and physical performance of marine coating systems (Reapproved 2011). West Conshohocken, PA.

Beltaos S, Rajaratnam N. 1974. Impinging circular turbulent jets. ASCE J Hydraul Div. 100:1313–1328.

Cassé F, Ribeiro E, Ekin A, Webster DC, Callow JA, Callow ME. 2007. Laboratory screening of coating libraries for algal adhesion. Biofouling. 23:267–276. doi:10.1080/08927010701288336

Cassé F, Swain GW. 2006. The development of microfouling on four commercial antifouling coatings under static and dynamic immersion. Int Biodeterior Biodegrad. 57:179–185. doi:10.1016/j.ibiod.2006.02.008

Demirel YK, Turan O, Incecik A. 2017. Predicting the effect of biofouling on ship resistance using CFD. Appl Ocean Res. 62:100–118. doi:10.1016/j.apor.2016.12.003

Donnelly B, Bedwell I, Dimas J, Scardino A, Tang Y, Sammut K. 2019. Effects of various antifouling coatings and fouling on marine sonar performance. Polymers. 11:614–663.

Earley PJ, Swope BL, Barbeau K, Bundy R, McDonald J. a, Rivera-Duarte I. 2014. Life cycle contributions of copper from vessel painting and maintenance activities. Biofouling. 30:51–68. doi:10.1080/08927014.2013.841891

Finlay JA, Callow ME, Schultz MP, Swain GW, Callow JA. 2002. Adhesion strength of settled spores of the green alga Enteromorpha. Biofouling. 18:251–256. doi:10.1080/08927010290029010

Finnie AA. 2006. Improved estimates of environmental copper release rates from antifouling products. Biofouling. 22:279–291. doi:10.1080/08927010600898862

Fischer M, Friedrichs G, Lachnit T. 2014. Fluorescence-based quasicontinuous and in situ monitoring of biofilm formation dynamics in natural marine environments. Appl Environ Microbiol. 80:3721–3728. doi:10.1128/AEM.00298-14

Gittens JE, Smith TJ, Suleiman R, Akid R. 2013. Current and emerging environmentally-friendly systems for fouling control in the marine environment. Biotechnol Adv. 31:1738–1753. doi:10.1016/j.biotechadv.2013.09.002

Haslbeck E, Ellor J. 2005. Investigating tests for antifoulants: variation between laboratory and in situ methods for determining copper release rates from navy-approved coatings. J Prot Coat Linings. 34–44.

Hearin J, Hunsucker KZ, Swain G, Gardner H, Stephens A, Lieberman K. 2016. Analysis of mechanical grooming at various frequencies on a large scale test panel coated with a fouling-release coating. Biofouling. 32:561–569. doi:10.1080/08927014.2016.1167880

Hearin J, Hunsucker KZ, Swain G, Stephens A, Gardner H, Lieberman K, Harper M. 2015. Analysis of long-term mechanical grooming on large-scale test panels coated with an antifouling and a fouling-release coating. Biofouling. 31(8):625–638. doi:10.1080/08927014.2015.1081687

Holm ER, Haslbeck EG, Horinek AA. 2003. Evaluation of brushes for removal of fouling from fouling-release surfaces, using a hydraulic cleaning device. Biofouling. 19:297–305. doi:10.1080/0892701031000137512

Howell D, Behrends B. 2006. A methodology for evaluating biocide release rate, surface roughness and leach layer formation in a TBT-free, self-polishing antifouling coating. Biofouling. 22:303–315. doi:10.1080/08927010600924304

Hunsucker KZ, Swain GW. 2016. In situ measurements of diatom adhesion to silicone-based ship hull coatings. J Appl Phycol. 28:269–277. doi:10.1007/s10811-015-0584-7

Hunsucker KZ, Vora GJ, Hunsucker JT, Gardner H, Leary DH, Kim S, Lin B, Swain G. 2018. Biofilm community structure and the associated drag penalties of a groomed fouling release ship hull coating. Biofouling. 34:111–162.

IMO. 2011. Guidelines for the control and management of ships' biofouling to minimize the transfer of invasive aquatic species. In: Resolut MEPC207(62). London (UK); p. 1–25.

ITTC. 2014. Recommended procedures and guidelines - 1978 ITTC performance prediction method 7.5-02-03-01.4 (Revision 03). Copenhagen (Denmark).

Kavanagh CJ, Schultz MP, Swain GW, Stein J, Truby K, Wood CD. 2001. Variation in adhesion strength of Balanus eburneus, Crassostrea virginica and Hydroides dianthus to fouling-release coatings. Biofouling. 17:155–167. doi:10.1080/08927010109378474

Kellett P, Mizzi K, Demirel YK, Turan O. 2015. Investigating the roughness effect of biofouling on propeller performance. In: International Conference on Shipping in Changing Climates, 2015–11–24 - 2015-11-26. Newcastle (UK): Technology and Innovation Centre.

Kiil S, Yebra DM. 2009. Modelling the design and optimization of chemically active marine antifouling coatings. In: Hellio C, Yebra D, editors, Advances in marine antifouling coatings and technologies. Cambridge (UK): Woodhead Publishing; p. 334–364.

Lagerström M, Lindgren JF, Holmqvist A, Dahlström M, Ytreberg E. 2018. In situ release rates of Cu and Zn from commercial antifouling paints at different salinities. Mar Pollut Bull. 127:289–296. doi:10.1016/j.marpolbul.2017.12.027

Larsson AI, Mattsson-Thorngren L, Granhag L, Berglin M. 2010. Fouling-release of barnacles from a boat hull with comparison to laboratory data of attachment strength. J Exp Mar Bio Ecol. 392:107–114. doi:10.1016/j.jembe.2010.04.014

Lejars M, Margaillan A, Bressy C. 2012. Fouling release coatings: a nontoxic alternative to biocidal antifouling

coatings. Chem Rev. 112:4347–4390. doi:10.1021/cr200350v

Lindholdt A, Dam-Johansen K, Olsen SM, Yebra DM, Kiil S. 2015. Effects of biofouling development on drag forces of hull coatings for ocean-going ships: a review. J Coat Technol Res. 12:415–444. doi:10.1007/s11998-014-9651-2

Lindholdt A, Dam-Johansen K, Yebra DM, Olsen SM, Kiil S. 2015. Estimation of long-term drag performance of fouling control coatings using an ocean-placed raft with multiple dynamic rotors. J Coat Technol Res. 12:975–995. doi:10.1007/s11998-015-9713-0

Malone JA. 1980. Effects of hull foulants and cleaning/coating practices on ship performances and economics. Trans - Soc Nav Archit Mar Eng. 88:75–101.

Menesses M, Belden J, Dickenson N, Bird J. 2017. Measuring a critical stress for continuous prevention of marine biofouling accumulation with aeration. Biofouling. 33:703–711. doi:10.1080/08927014.2017.1359574

Montgomery DC. 2013. Design and analysis of experiments. 8th ed. Singapore: John Wiley and Sons, Inc.

Morrisey D, Woods C. 2015. In-water cleaning technologies: review of information Prepared for Ministry for Primary Industries. Wellington (New Zealand): Ministry of Primary Industries.

Morrisey D, Woods CMC, Bell A, Georgiades E. 2013. In-water cleaning of vessels: biosecurity and chemical contamination risks. Wellington (New Zealand): Ministry of Primary Industries.

Murphy EAK, Barros JM, Schultz MP, Flack KA, Steppe CN, Reidenbach MA. 2018. Roughness effects of diatomaceous slime fouling on turbulent boundary layer hydrodynamics. Biofouling. 34(9):976–988. DOI: doi:10.1080/08927014.2018.1517867.

Naval Sea Systems Command. 2006. Chapter 081 – Waterborne underwater hull cleaning of Navy ships. In: Nav Ship's Tech Man. Washington (DC).

Oliveira D, Granhag L. 2016. Matching forces applied in underwater hull cleaning with adhesion strength of marine organisms. J Mar Sci Eng. 4:66–78. doi:10.3390/jmse4040066

Oliveira DR, Larsson L, Granhag L. 2019. Towards an absolute scale for adhesion strength of ship hull microfouling. Biofouling. 35:244–258. doi:10.1080/08927014.2019.1595602

Park JS, Lee JH. 2018. Sea-trial verification of ultrasonic antifouling control. Biofouling. 34(1):98–110. DOI: doi:10.1080/08927014.2017.1409347.

Sanchez A, Yebra DM. 2009. Ageing tests and long-term performance of marine antifouling coatings. In: Hellio C, Yebra D, editors, Advances in marine antifouling coatings and technologies. Cambridge (UK): Woodhead Publishing; p. 393–421.

Schiff K, Diehl D, Valkirs A. 2004. Copper emissions from antifouling paint on recreational vessels. Mar Pollut Bull. 48:371–377. doi:10.1016/j.marpolbul.2003.08.016

Schultz MP. 2007. Effects of coating roughness and biofouling on ship resistance and powering. Biofouling. 23:331–341. doi:10.1080/08927010701461974

Schultz MP, Bendick JA, Holm ER, Hertel WM. 2011. Economic impact of biofouling on a naval surface ship. Biofouling. 27:87–98. doi:10.1080/08927014.2010.542809

Schultz MP, Finlay JA, Callow ME, Callow JA. 2000. A turbulent channel flow apparatus for the determination of the adhesion strength of microfouling organisms. Biofouling. 15:243–251. doi:10.1080/08927010009386315

Scianni C, Georgiades E. 2019. Vessel in-water cleaning or treatment: identification of environmental risks and science needs for evidence-based decision making. Front Mar Sci. 6:1–12.

SMHI. 2019. Swedish Meteorological and Hydrological Institute's database of historical oceanographic observations: sea temperature and tides [Internet]. [cited 2019 Apr 2]. Available from: https://www.smhi.se/klimatdata/oceanografi/ladda-ner-oceanografiska-observationer.

Swain GW, Lund G. 2016. Dry-dock inspection methods for improved fouling control coating performance. J Sh Prod Des. 32:1–8.

Swain GW, Schultz MP. 1996. The testing and evaluation of non-toxic antifouling coatings. Biofouling. 10:187–197. doi:10.1080/08927019609386279

Townsin RL. 2012. A note on hull roughness measurement surveys. TQC [Internet]. [cited 2019 Sep 9]. Available from: https://www.hull-roughness.com/a-note-on-hull-roughness-measurement-surveys.

Tribou M, Swain G. 2017. The effects of grooming on a copper ablative coating: a six year study. Biofouling. 33:494–504. doi:10.1080/08927014.2017.1328596

Tribou M, Swain GW. 2010. The use of proactive in-water grooming to improve the performance of ship hull antifouling coatings. Biofouling. 26:47–56. doi:10.1080/08927010903290973

Tribou M, Swain GW. 2015. Grooming using rotating brushes as a proactive method to control ship hull fouling. Biofouling. 31:309–319. doi:10.1080/08927014.2015.1041021

Watermann BT, Daehne B, Sievers S, Dannenberg R, Overbeke JC, Klijnstra JW, Heemken O. 2005. Bioassays and selected chemical analysis of biocide-free antifouling coatings. Chemosphere. 60:1530–1541. doi:10.1016/j.chemosphere.2005.02.066

Woods Hole Oceanographic Institute. 1952. Marine fouling and its prevention. Menasha (WI): George Banta Publishing Co.

Yebra DM, Kiil S, Dam-Johansen K. 2004. Antifouling technology - past, present and future steps towards efficient and environmentally friendly antifouling coatings. Prog Org Coat. 50:75–104. doi:10.1016/j.porgcoat.2003.06.001

Zargiel KA, Swain GW. 2014. Static vs dynamic settlement and adhesion of diatoms to ship hull coatings. Biofouling. 30:115–129. doi:10.1080/08927014.2013.847927